Azide Binding Controlled by Steric Interactions in Second Sphere. Synthesis, Crystal Structure, and Magnetic Properties of [Ni II 2 (L)(μ 1,1 -N 3)][ClO 4] (L = Macrocyclic N 6 S 2 Ligand)

Alexander Jeremies, Sina Gruschinski, Michel Meyer, Vitaly Matulis, Oleg A. Ivashkevich, Karolin Kobalz, Berthold Kersting

Azide Binding Controlled by Steric Interactions in Second Sphere. Synthesis, Crystal Structure, and Magnetic Properties of $[Ni^{II}_2(L)(\mu_{1,1}\text{-}N_3)][ClO_4]$ (L = Macrocyclic N_6S_2 Ligand)

Alexander Jeremies,[a] Sina Gruschinski,[a] Michel Meyer,*[,b] Vitaly Matulis,[c] Oleg A. Ivashkevich,[d] Karolin Kobalz,[a] and Berthold Kersting*[,a]

[a] *Institut für Anorganische Chemie, Universität Leipzig, Johannisallee 29, 04103 Leipzig, Germany,* E-mail: b.kersting@uni-leipzig.de, Fax: +49/(0)341-97-36199

[b] *Institut de Chimie Moléculaire de l'Université de Bourgogne (ICMUB), UMR 6302, CNRS, Université Bourgogne-Franche Comté, 9 avenue Alain Savary, BP 47870, 21078 Dijon Cedex, France,* E-mail: michel.meyer@u-bourgogne.fr, Fax: +33/(0)3 80 39 61 17

[c] *Research Institute for Physical Chemical Problems of Belarusian State University, Leningradskaya 14, 220030 Minsk, Belarus*

[d] *Belarusian State University, 4 Nezavisimisti avenue, 220050 Minsk, Belarus*

Published on February 2, 2016 as an article in

Inorganic Chemistry **2016**, *55*, 1843–1853

DOI: 10.1021/acs.inorgchem.5b02743

* Corresponding author.

Abstract

The dinuclear Ni^{II} complex $[Ni_2(L^2)][ClO_4]_2$ (**3**) supported by the 28-membered hexaaza-dithiophenolate macrocycle $(L^2)^{2-}$ binds the N_3^- ion specifically *end-on* yielding $[Ni_2(L^2)(\mu_{1,1}\text{-}N_3)][ClO_4]$ (**7**) or $[Ni_2(L^2)(\mu_{1,1}\text{-}N_3)][BPh_4]$ (**8**), while the previously reported complex $[Ni_2L^1(\mu_{1,3}\text{-}N_3)][ClO_4]$ (**2**) of the 24-membered macrocycle $(L^1)^{2-}$ coordinates it in the *end-to-end* fashion. A comparison of the X-ray structures of **2**, **3**, and **7** reveals the form-selective binding of complex **3** to be a consequence of its pre-organized, channel-like binding pocket, which accommodates the azide anion via repulsive CH···π interactions in the *end-on* mode. In contrast to $[Ni_2L^1(\mu_{1,3}\text{-}N_3)][ClO_4]$ (**2**), which features a $S = 0$ ground state, $[Ni_2(L^2)(\mu_{1,1}\text{-}N_3)][BPh_4]$ (**8**) has a $S = 2$ ground state that is attained by competing antiferromagnetic and ferromagnetic exchange interactions via the thiolato and azido bridges with a value for the magnetic exchange coupling constant J of 13 cm^{-1} ($\mathbf{H} = -2JS_1S_2$). These results are further substantiated by DFT calculations. The stability of the azido-bridged complex determined by isothermal titration calorimetry in MeCN/MeOH 1/1 v/v ($\log K_{11} = 4.88(4)$ at $I = 0.1$ M) lies in between those of the fluorido- ($\log K_{11} = 6.84(7)$) and chlorido-bridged complexes ($\log K_{11} = 3.52(5)$). These values were found to compare favorably well with the equilibrium constants derived at lower ionic strength ($I = 0.01$ M) by absorption spectrophotometry ($\log K_{11} =$ 5.20(1), 7.77(9), and 4.13(3) for N_3^-, F^-, and Cl^- respectively).

Introduction

The magnetochemistry of polynuclear nickel complexes with bridging azido ligands has been extensively investigated due to the fact that the azide bridges efficiently mediate magnetic exchange between the unpaired electrons of the paramagnetic metal ions.[1,2] The *end-on* and *end-to-end* modes are frequently encountered in dinuclear complexes,[3] but triply bridging[4,5] or quadruply bridging modes[6-8] have also been reported for some tetranuclear complexes. The *end-on* bridging mode ($\mu_{1,1}$) usually provides a ferromagnetic coupling between the Ni^{II} ions, while the *end-to-end* mode ($\mu_{1,3}$) enables a pathway for an antiferromagnetic exchange interaction. Thus, control of the azide binding mode can dictate the properties of molecular-based magnetic materials.[9] However, the coordination behavior of the azide ion is difficult to control[10-12] and has been achieved only in a few cases.[13] Beer *et al.*, for example, have appended two triazacyclononane rings (tacn) on a calixarene backbone and the three bridging azido ligands in the corresponding Ni_2 complex all act as *end-on* bridges.[14] This compound should be compared with the unmodified $[(Me_3tacn)_2Ni_2(N_3)_3]^+$ system, which appears in three forms, one with three *end-on* bridges as in Beer's compound,[10] one form with three *end-to-end* bridges,[15] and the third one with only two *end-to-end* bridges. In another relevant study, Escuer *et al.* used a dinuclear cryptate of ellipsoidal shape to enforce the *end-to-end* mode in a Ni^{II} complex.[16] The same binding mode is also present in dinuclear bis-tren-based coordination cages reported by Fabbrizzi and Favarelli.[17]

The coordination chemistry of the 24-membered dinucleating hexaaza-dithiophenolate macrocycle $(L^1)^{2-}$ (Figure 1) has been investigated in much detail.[18] The macrocycle can adopt two conformations A and B, reminiscent of the "partial cone" and "cone" conformations of the calixarenes. In the case of Ni^{2+}, the type A conformation is only seen for small monoatomic bridging ligands, as for instance in $[Ni_2(L^1)(\mu\text{-Cl})][BPh_4]$ (**1**).[19] For multiatom bridging ligands the bowl-shaped conformation B is assumed. The complex $[Ni_2(L^1)(\mu_{1,3}\text{-}N_3)][ClO_4]$ (**2**), with the azide ion in the *end-to-end* mode, is a representative

example.[20] This complex is characterized by an antiferromagnetic exchange interaction (J = –45.6 cm^{-1}; **H** = $-2JS_1S_2$).

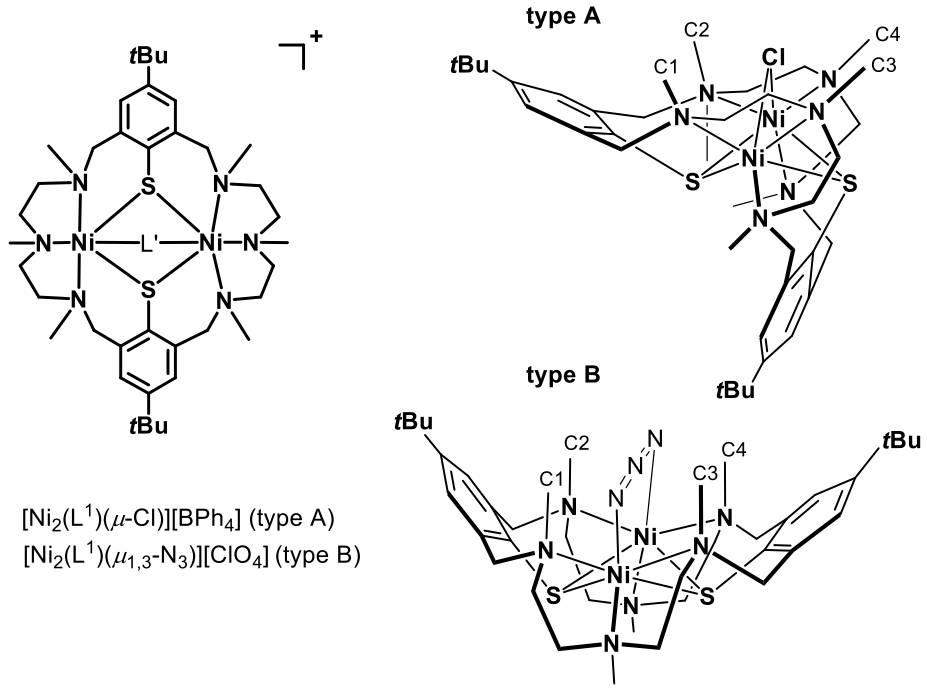

Figure 1. Complexes **1** and **2** supported by the macrocycle $(L^1)^{2-}$ and representation of the two possible conformations of type A and B referred to in the text. In each case, four methyl groups (labeled C1–C4) surround the co-ligands. The intramolecular C···C distances define the size of the binding pocket (C1···C2, C1···C3, C2···C4, C3···C4 = 4.290, 4.113, 4.253, 5.292 Å (**1**); 7.274, 3.574, 3.504, 7.335 Å (**2**)).

More recently, we have reported some dinickel complexes of a 28-membered variant of $(L^1)^{2-}$, which contains propylene groups in place of the ethylene linkers in the lateral side arms (Figure 2).[21] In contrast to $(L^1)^{2-}$, only few dinuclear nickel complexes are supported with $(L^2)^{2-}$. So far only the parent complex $[Ni_2(L^2)][ClO_4]_2$ (**3**) and the halido-bridged $[Ni_2(L^2)(\mu\text{-Hal})][ClO_4]$ species (Hal = F$^-$ (**4**), Cl$^-$ (**5**), Br$^-$ (**6**)) have been reported.[22] In these compounds, the macrocycle invariably adopts a conformation of type C (Figure 2),[21] which is similar but not identical to the type A conformation in **1**. In the latter, the Cl$^-$ ligand is

surrounded by four methyl groups, while two propylene chains (marked in red) surround the active coordination site in **3**–**6**. A detailed structural analysis revealed that the reluctance of **3** to accommodate further bridging ligands is a consequence of a high degree of pre-organization of the $[Ni_2(L^2)]^{2+}$ receptor and a size fit mismatch of the receptors binding cavity for anions much larger than F^-.[21]

In this paper, we report on the successful synthesis and characterization of the azido-bridged complexes $[Ni_2(L^2)(\mu_{1,1}\text{-}N_3)][ClO_4]$ (**7**) and $[Ni_2(L^2)(\mu_{1,1}\text{-}N_3)][BPh_4]$ (**8**). The form-selective binding of the azide ion in the *end-on* mode is demonstrated, as is the switch of the magnetic exchange interaction from antiferromagnetic in **2** to ferromagnetic in **8**. The results of broken-symmetry DFT calculations, UV- spectroscopic titrations and isothermal calorimetry measurements are also reported.

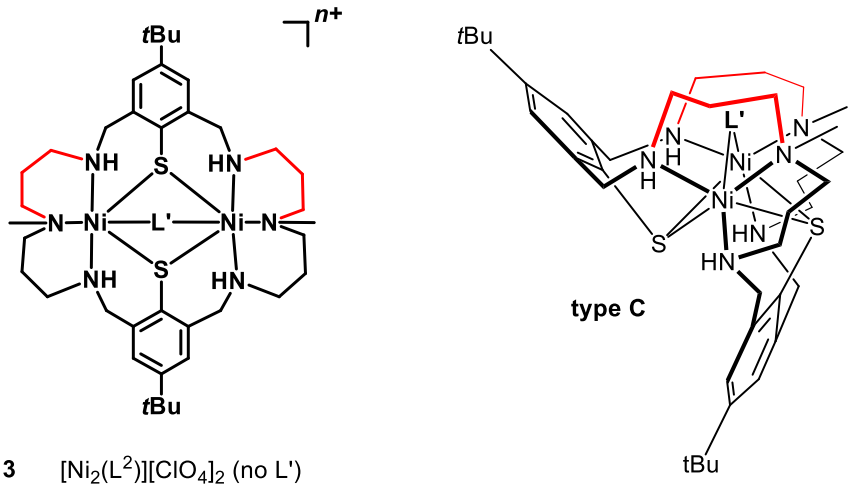

3 $[Ni_2(L^2)][ClO_4]_2$ (no L')
4–6 $[Ni_2(L^2)(\mu\text{-Hal})][ClO_4]$ (Hal = F^-, Cl^-, Br^-)
7 $[Ni_2(L^2)(\mu_{1,1}\text{-}N_3)][ClO_4]$
8 $[Ni_2(L^2)(\mu_{1,1}\text{-}N_3)][BPh_4]$

Figure 2. Complexes **3**–**8** supported by the macrocycle $(L^2)^{2-}$ and representation of the structure of the "type C" conformation referred to in the text.

Results and Discussion

Synthesis and Characterization of Complexes 7 and 8. Treatment in methanol of dark-green $[Ni_2(L^2)][ClO_4]_2\cdot 2H_2O$ (**3**·2H_2O) with N(*n*-Bu)$_4N_3$ in a 1:1 molar ratio immediately

affords a pale-green solution, from which a brown perchlorate salt of composition $[Ni_2(L^2)(\mu\text{-}N_3)][ClO_4]_2\cdot H_2O$ (**7**·H_2O) could be reproducibly isolated in yields as high as 87% (eq 1a). Anion metathesis of **7**·H_2O with $NaBPh_4$ in MeOH provides the corresponding tetraphenylborate salt **8**·H_2O (eq 1b). Isolated **7**·H_2O and **8**·H_2O are moderately soluble in polar protic solvents, but are highly soluble in MeCN, DMF, and DMSO. The compounds gave satisfactory elemental analysis assuming the presence of one co-crystallized water molecule, while the molecular peaks in the ESI-MS spectra of both **7** and **8** confirm the presence of the $[Ni_2(L^2)(\mu\text{-}N_3)]^+$ cation (*m/z* = 826.3).

$$[Ni_2(L^2)][ClO_4]_2 + N(n\text{-}Bu)_4N_3 \longrightarrow [Ni_2(L^2)(\mu_{1,1}\text{-}N_3)][ClO_4] + N(n\text{-}Bu)_4ClO_4 \quad (1a)$$

3 **7**

$$[Ni_2(L^2)(\mu_{1,1}\text{-}N_3)][ClO_4] + NaBPh_4 \longrightarrow [Ni_2(L^2)(\mu_{1,1}\text{-}N_3)][BPh_4] + NaClO_4 \quad (1b)$$

7 **8**

Crystal Structure of Complex 7·5EtOH. X-ray diffraction analysis of crystals of **7**·5EtOH grown by slow evaporation from a MeOH/MeCN solution clearly confirmed the presence of an *end-on* azido bridge. Figure 3 shows the structure of the $[Ni_2(L^2)(\mu_{1,1}\text{-}N_3)]^+$ cation, along with that of its precursor **3** reported previously.[21] Table S1 (Supporting Information) lists selected bond lengths and angles.

The conformation of the macrocycle in the parent complex **3**[21] is largely retained upon azide binding, but the average Ni–N and Ni–S distances increase both by 0.07 Å, as one might expect from the increase of the coordination number from five in **3** to six in **7**. With respect to the magnetic properties (see below), the decrease of the average Ni–S–Ni angle from 89(2)° in **3**, to 81.5(2)° in **7**, may also be noted. The N_3^- is almost linear (N–N–N = 178.4°) but asymmetric in terms of the N–N distances (1.186(6), 1.167(8) Å). Likewise, the Ni–N(azide) bond distances (2.231(5) and 2.219(3) Å) and the Ni–N_3–Ni angle (92.9(1)°) deviate significantly from the expected values. In other triply bridged structures with *end-on*

azido ligands, the bond lengths are much smaller (~ 2.1 Å) and the angles are much more acute (<86°).[11,14] The binding site in **7** is obviously not perfectly pre-organized for a $\mu_{1,1}$-bridging azide ion. We have not been able to grow single crystals of the tetraphenylborate salt **8**. On the basis of the spectroscopic data, the $[Ni_2(L^2)(\mu_{1,1}\text{-}N_3)]^+$ cation in the tetraphenylborate salt is assumed to be isostructural with that in the perchlorate salt **7**.

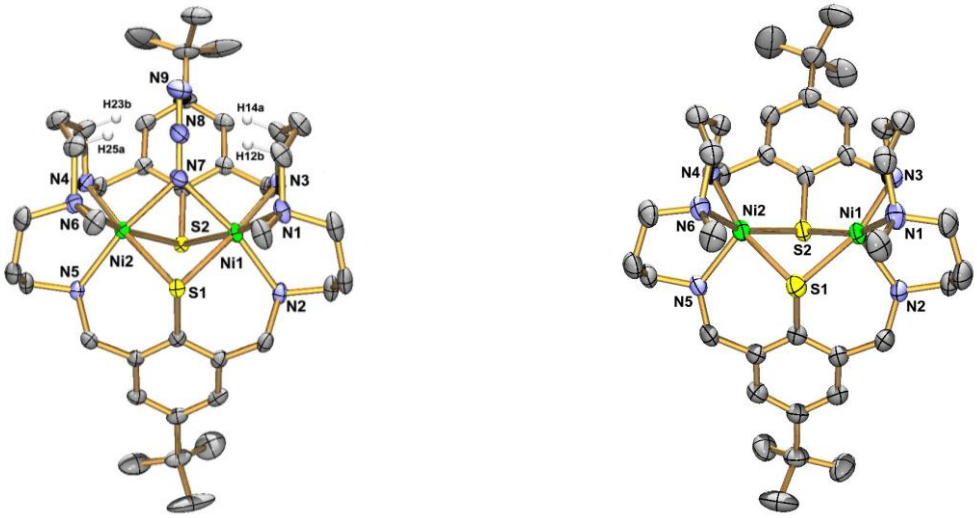

Figure 3. Ortep representations of the molecular structures of the $[Ni_2(L^2)(\mu_{1,1}\text{-}N_3)]^+$ cation in crystals of **7**·5EtOH (left, most hydrogen atoms are omitted for sake of clarity) and of $[Ni_2(L^2)]^+$ in the parent complex **3**·4EtOH (right)[21] for comparison. Ellipsoids are drawn at the 30% probability level.

The short distances between the N_3^- ion and the surrounding CH_2 groups of the macrocycle merit consideration. All four hydrogen atoms labeled H12b, H14a, H23b, and H25a point to the central atom N8 of the azide ion. The corresponding H···N8 distances range from 2.305 to 2.396 Å, respectively. These values are significantly smaller than the sum of the van der Waals radii of the two elements (2.75 Å).[23,24] In Escuer's cryptate complex, the intramolecular distances between the encapsulated azide ion and the surrounding benzene rings are much longer (2.9–3 Å).[16] The distances between the opposing C atoms of the two propylene linkers (C14···C23 and C12···C25) should also be taken into account. These increase significantly

from 4.704 Å in **3** to 5.678 Å in **7**, suggesting the presence of repulsive interactions between the propylene linkers and the azide ion. However, according to the IR data, there is no indication for blue-shifting CH···π hydrogen bonding interactions (*vide infra*).[25] Nevertheless, the selective binding of the azide ion is clearly governed by the propylene chains, which form a narrow pocket about the complexes' binding site. It should be noted in this respect that coordination of the azide ion does not affect the conformation of the macrocycle, which is that of type C as found for the receptor **3** or the halido-bridged complexes **4**–**6**. The analogous complexes **1** and **2** of the 24-membered macrocycle adopt two different conformations A and B (Figure 2), indicative of a lower level of pre-organization.

Figure 4 displays the intermolecular hydrogen bonding interactions involving the $[Ni_2(L^2)(\mu_{1,3}\text{-}N_3)]^+$ cation and the ClO_4^- ion. As can be seen, one of the secondary amine function acts as a H donor towards a ClO_4^- ion, with N···O distances ranging from 3.065 to 3.305 Å. The other NH donors are in the vicinity of the solvent accessible voids determined with the SQUEEZE procedure implemented in the PLATON program suite.[26] This suggests that the other three NH donors are involved in H bonding interactions with the EtOH solvates as well. There is no void about the terminal N9 atom of the azide ion, which corroborates its lipophilic behavior.[27] The closest distance is that of a CH_2 group of a symmetry related $[Ni_2(L^2)(\mu_{1,1}\text{-}N_3)]^+$ cation at 3.995 Å (N9···H24').

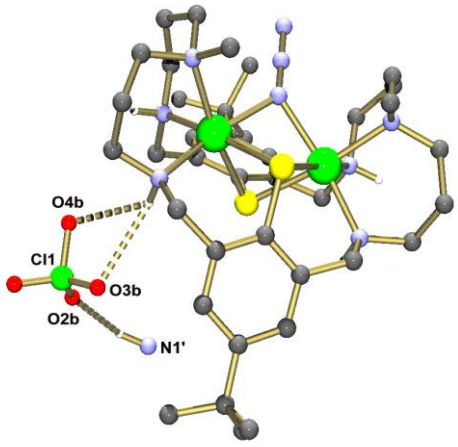

Figure 4. Intermolecular hydrogen bonding interactions between the $[Ni_2(L^2)(\mu_{1,1}\text{-}N_3)]^+$ cation and the ClO_4^- anion in crystals of **7**·5EtOH. Thermal ellipsoids are drawn at the 30% probability level. Most hydrogen atoms are omitted for sake of clarity. Only one orientation of the disordered ClO_4^- ion is shown. Selected bond lengths: N6···O3b = 3.305, N6···O4b = 3.280, O2b···N1' = 3.065 Å. Symmetry code used to generate equivalent atoms: *x*, 0.5–*y*, 0.5+z (').

Magnetic Properties of Complexes 3 and 8. To get an insight into the magnetic properties of the azido-bridged complexes, variable-temperature magnetic susceptibility data were measured for **3**·2H_2O and **8**·H_2O between 2 and 330 K in an applied external magnetic field of B = 0.5 T. Figure 5 shows the susceptibility data (per binuclear complex) in the form of μ_{eff} versus T plots. For complex **3**, the effective magnetic moment per binuclear complex at 300 K (4.10 μ_B) is smaller than the expected value of 4.40 μ_B calculated for two non-interacting Ni^{II} (S = 1) ions having reasonable g values of 2.2. With decreasing temperature the values constantly decrease to a minimum of 0.43 μ_B at 2 K. This behavior indicates the presence of an intramolecular antiferromagnetic exchange interaction that leads to a S_t = 0 ground state.

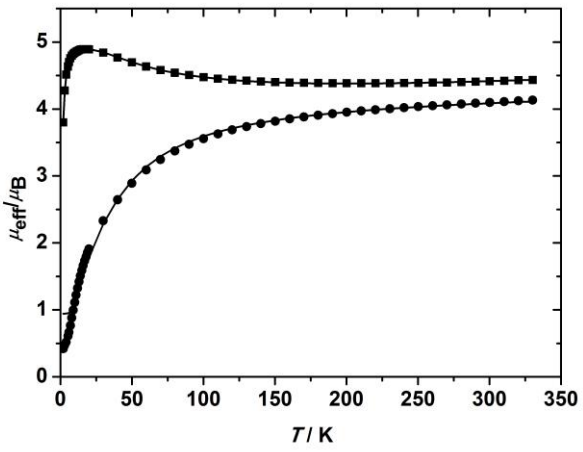

Figure 5. Temperature dependence of the effective magnetic moment μ_{eff} (per dinuclear complex) for **3** (●) and **8** (■). The full lines represent the best fits to eq 2.

Complex **8** shows different magnetic properties. Indeed, the effective magnetic moment increases from 4.44 μ_B at 300 K to a maximum value of 4.89 μ_B at 17 K. On lowering the temperature further the magnetic moment decreases to 3.80 μ_B at 2 K. This behavior is indicative for an intramolecular ferromagnetic exchange interaction between the two nickel(II) ions that leads to a $S_t = 2$ ground state. The decrease in $\chi_M T$ below 20 K can be attributed to zero-field splitting of Ni^{II}.[28] It is clear that the change of the coupling type from antiferromagnetic in **3** to ferromagnetic in **8** is in large part due to the accommodation of the $\mu_{1,1}$-bridging N_3^- ion.

In both compounds, the two ions differ slightly and none is axial, so the appropriate spin-Hamiltonian (eq 2)[29] would include additional terms to account for single-ion zero-field splitting for each Ni^{2+} ion (e.q. 2a). J is the exchange coupling constant, D_i, E_i/D_i, and g_i are the local axial and rhombic zero field splitting parameters and g values (isotropic average).[30] However, temperature dependent magnetic susceptibility measurements are not very appropriate for the determination of the sign and magnitude of D,[31] and so the data were analyzed with the approximation in eq. 2b, using a full-matrix diagonalization approach.[32] To reduce the number of variables the D and g values were considered to be identical for the two nickel atoms.

$$H = -2JS_1S_2 + \sum_{i=1}^{2} D_i\left[S_{z,i}^2 - \frac{1}{3}S_i(S_i+1) + \frac{E_i}{D_i}(S_{x,i}^2 - S_{y,i}^2)\right] + g_i\mu_B B_\tau \hat{S}_{i,\tau} \qquad (2a)$$


($\tau = x, y, z$) (2b)

By taking into account the zero-field splitting and temperature independent paramagnetism (TIP), reasonable fits of the experimental data shown in Figure 5 as solid lines were possible,

yielding $J = -15$ cm^{-1} ($g = 2.18$, $D = 0.0035$ cm^{-1}) for **3** and $J = +13$ cm^{-1} ($g = 2.18$ (fixed), $D = 8.46$ cm^{-1}) for **8**. The inclusion of the D parameter improved the low-temperature fits significantly, but as stated above, these values represent by no means accurate values.[33] Nevertheless, the value of J is unambiguous and represents an accurate measure of the magnetic coupling in **3** and **8**. The experimental *J* values agree also reasonably well with those obtained by broken symmetry density functional calculations for exchange interactions ($J = -7.40$ cm^{-1} for **3**; $J = +23.18$ cm^{-1} for **8**, Table 1).

It is interesting to compare the magnetic properties of complex **8** with that of complex **2**, since their main structural difference is the azide-bridging mode. The structure and magnetic properties of **2** have been determined previously (Table 1).[20] In contrast to **8**, this complex features a $\mu_{1,3}$-bridging azido ligand and has a $S_{tot} = 0$ ground state that is attained by an antiferromagnetic exchange interaction between the two Ni^{2+} ions ($S = 1$). Notice also that the magnitude of the coupling in **2** ($J = -45.6$ cm^{-1}) is significantly stronger than in **3** ($J = -15$ cm^{-1}).

Table 1. Magnetic Properties of Selected Dinickel Complexes with Edge-Sharing Bis-square-pyramidal $N_3Ni(\mu\text{-}SR)_2NiN_3$ (**3**, **7'**) and Bisoctahedral $N_3Ni(\mu\text{-}SR)_2(\mu\text{-}L')NiN_3$ Cores (L' = N_3^-, **2**, **2'**, **7**, **8**)

	complex	Ni···Ni (Å)	Ni–S–Ni (°)	J_{exp} (cm^{-1})	J_{DFT} (cm^{-1})	*g*	Ref.
2	$[Ni_2(L^1)(\mu_{1,3}\text{-}N_3)][ClO_4]$	n.d.[a]	n.d.[a]	–45.6	n.d.[a]	2.25	[20]
2'	$[Ni_2(L^1)(\mu_{1,3}\text{-}N_3)][N_3]$	3.684(1)	94.6(5)	n.d.[a]	–56.48	n.d.	[20]
3	$[Ni_2(L^2)][ClO_4]_2$	3.369(4)	89(2)	–15	–7.40[b]	2.18	This work
7	$[Ni_2(L^2)(\mu_{1,1}\text{-}N_3)][ClO_4]$	3.226(1)	81.81	n.d.	n.d.	n.d.	This work
7'	$[Ni_2(L^2)]^{2+}$	3.226(1)	81.81	–	–21.93[b,c]	n.d.	This work
8	$[Ni_2(L^2)(\mu_{1,1}\text{-}N_3)][BPh_4]$	n.d.	n.d.	+13	+23.18[b]	2.18 (fixed)	This work

[a] Crystals of **2** could not be obtained. However, crystals of the azide salt $[Ni_2(L^1)(\mu_{1,3}\text{-}N_3)][N_3]$ (**2'**) were suitable for X-ray structure analysis. On the basis of spectroscopic data, the $[Ni_2(L^1)(\mu_{1,3}\text{-}N_3)]^+$ cations in **2** and **2'** are deemed structurally identical. Magnetic measurements were performed for the perchlorate salt $[Ni_2(L^1)(\mu_{1,3}\text{-}N_3)][ClO_4]$ (**2**). DFT calculations are based on the X-ray structure for the cation in **2'**. [b] Density functional *J*

values were computed in this work at the PBE0/TZV(P) level of theory with relativistic effects. [c] DFT calculations are based on the X-ray structure for the cation in **7** (with the N_3^- ion omitted).

The comparison of the magnetic properties of **2**, **3**, and **8** implies that the coupling through the two thiolato-bridges is in all cases antiferromagnetic in nature. This fact is not only corroborated by experiment but also by computations on model complexes (Table 1), where a breakdown approach was applied in order to evaluate the coupling through the dissimilar bridges.[34] Thus, removing virtually the azido group from **8**, yields the dication $[Ni_2(L^2)]^{2+}$ (**7'**), for which the *J* value was calculated to be –21.93 cm^{-1}. If it can be assumed that the overall coupling is the arithmetic sum of the coupling through the two thiolato and azido-bridges, this would then lead to the conclusion that competing antiferromagnetic and ferromagnetic exchange interactions are present in **8**. A larger "ferromagnetic" contribution of 45.11 cm^{-1} through the $\mu_{1,1}$-bridging N_3^- ion would then override the smaller antiferromagnetic interaction through the thiolato-bridges, to produce a change in the sign of *J*. There are not many examples in the literature with which this kind of complexes can be compared. Ruiz and co-workers have performed DFT calculations on various model complexes.[35] The *J* values were found to depend primarily on the bridging angle θ and the Ni–N distance. For $[Ni_2(\mu_{1,1}\text{-}N_3)_2(NH_3)_8]^{2+}$, *J* ranged between 60 cm^{-1} for $\theta \approx 90°$ to a maximum value of 80 cm^{-1} at $\theta \approx 104°$. Considering that the calculated *J* values are overestimated by a factor of 2,[35] our value is in very good agreement with the reported trend.

Infrared and Raman Spectroscopy. Figure 6 displays the FT-MIR spectra of **7**·H_2O and **8**·H_2O in the 2000–2200 cm^{-1} region. That of **2** is also shown for comparison. As can be seen, a strong IR allowed but Raman forbidden band attributable to the $\nu_{asym}(N_3^-)$ stretching frequency appears at 2041 cm^{-1}, a value typical for $\mu_{1,1}$-azido linkages.[36,37] Relative to **2** (2059 cm^{-1}), this band is significantly red-shifted (Δ = 18 cm^{-1}), owing to the switch of the

coordination mode from *end-to-end* in **2** to *end-on* in **7** and **8**. In Raman spectroscopy only the symmetrical vibration mode of N_3^- is allowed and appears at 1297 and 1303 cm^{-1} for **7**·H_2O and **8**·H_2O, respectively. As revealed by the crystal structure, the CH_2 groups and the N_3^- ion are in close contact, and so the CH_2 region was screened for possible blue-shifting $CH_2\cdots\pi(N_3^-)$ hydrogen bonding interactions.[25] However, the values are quite normal for CH_2 groups. The $\nu_{sym}(CH_2)$ stretches in **7** and **8** are somewhat broadened, have a higher intensity, and are red-shifted by ~7 cm^{-1} when compared with those of **3**.

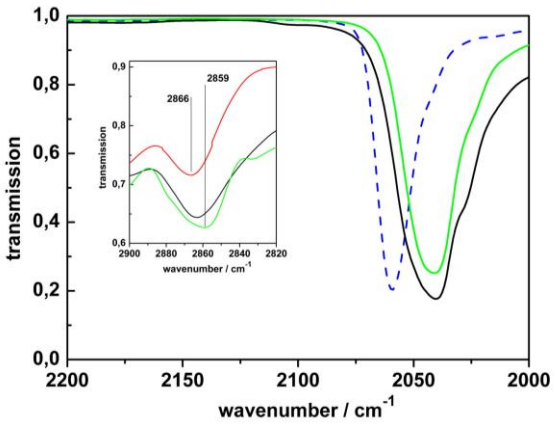

Figure 6. Section of the IR spectra of $[Ni_2(L^2)(\mu_{1,1}\text{-}N_3)][ClO_4]\cdot H_2O$ (**7**·H_2O, black solid line), $[Ni_2(L^2)(\mu_{1,1}\text{-}N_3)][BPh_4]\cdot H_2O$ (**8**·H_2O, green line), and $[Ni_2(L^1)(\mu_{1,3}\text{-}N_3)][ClO_4]$ (**2**, dashed blue line). The inset shows the IR spectra of $[Ni_2(L^2)][ClO_4]_2\cdot 2H_2O$ (**3**·$2H_2O$, red line), **7**·H_2O (black), and **8**·H_2O (green) from 2820 to 2900 cm^{-1}.

UV–vis–NIR Spectroscopy. The absorption spectrum of the deep-green colored precursor complex **3**·$2H_2O$ in neat acetonitrile (Figure 7) is characterized by four visible absorption bands at 531, 635, 786, and 1012 nm (the corresponding band assignment can be found in Table 2), as typically observed for Ni^{2+} centers in a square-pyramidal N_3S_2 environment.[21] In turn, solutions of **7**·H_2O and **8**·H_2O in the same solvent are pale-green and reveal two absorption bands at 645 and 1020 nm attributable to *d*–*d* transitions ($\nu_2(^3A_{2g} \rightarrow {}^3T_{1g})$ and

$\nu_1(^3A_{2g} \rightarrow {}^3T_{2g})$) for a distorted octahedral $Ni^{II}N_3S_2(N_3)$ chromophore. The spin-forbidden $^3A_{2g} \rightarrow {}^1E_g$ (D) transition, which gains intensity owing to the deviation from pure octahedral symmetry, gives rise to a shoulder close to 914 nm as the corresponding band strongly overlaps with the ν_1 band. When compared to the free receptor **3** in which both metal centers are pentacoordinated, the marked hypochromicity of **7** and **8** is in line with the increase in coordination number and the more symmetrical arrangement of the donor atoms. Moreover, it also clearly evidences the stability of the supramolecular host-guest assembly in solution. Addition of 50% of methanol in the medium does not affect the electronic properties of the complex (Table 1), indicating a similar coordination environment in both solvents without significant dissociation and release of free azide (the molar fractions of **3** and free N_3^- reach ~7% for a 10^{-3} M solution of **7**·H_2O in MeCN/MeOH (50/50 v/v), *vide infra*). Noteworthy, the diffuse reflectance spectrum of a microcrystalline sample of **7**·H_2O (Figure S1) is slightly red-shifted (by 28 and 49 nm for ν_2 and ν_1, respectively) with respect to the solution spectrum, suggesting that the central thiolato-bridged $Ni^{II}N_3S_2(N_3)$ core experiences some slight structural rearrangements upon dissolution. If one refers to the H-bond network involving the secondary amines of $(L^2)^{2-}$, perchlorate counter anion, and the co-crystalized solvent molecules seen in the crystal structure (Figure 4), a somewhat weaker ligand field might be anticipated in the solid state owing to Ni–N bond elongation. Likewise, the solvent-induced breakage of these hydrogen bonds should also logically induce in a slight structural reorganization. Noteworthy, this seems not to be the case for compound **3**·$2H_2O$ (Table 2, Figure S1), for which both solid-state and solution structures are essentially identical.[21]

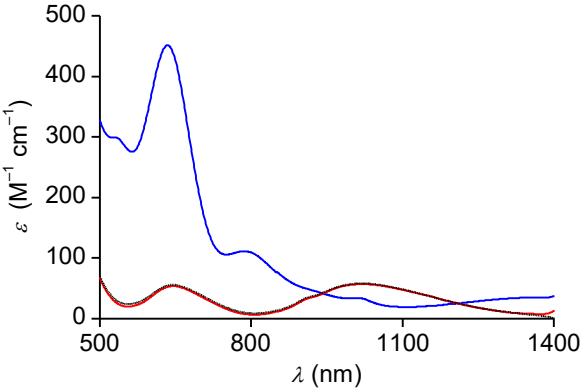

Figure 7. UV–vis–NIR spectra of $[Ni_2(L^2)][ClO_4]_2 \cdot 2H_2O$ (**3**·2H₂O, blue line), $[Ni_2(L^2)(\mu_{1,1}\text{-}N_3)][ClO_4] \cdot H_2O$ (**7**·H₂O, red line), and $[Ni_2(L^2)(\mu_{1,1}\text{-}N_3)][BPh_4] \cdot H_2O$ (**8**·H₂O, black dashed line) in CH_3CN. Concentration of solutions: 10^{-3} M.

From the difference in colors between **7**·H₂O (pale-green/brown) and **8**·H₂O (pale-green), it is already obvious that the counter anion exerts some influence on the chromophore and thus on the ligand-field strength. Replacing ClO_4^-, which is prone to form hydrogen-bonds with surrounding H-donors, by a bulkier and inert BPh_4^- anion as in **8**·H₂O results in a significant hypsochromic shift of both ν_2 ($\Delta\lambda$ = 27 nm) and ν_1 ($\Delta\lambda$ = 66 nm) absorption bands in the powder spectrum (additional strong features are found at 269, 311, and 392 nm for **8**·H₂O, Figure S1). In contrast to the solid perchlorate salt, the higher ligand field strength of $(L^2)^{2-}$ in the tetraphenylborate analog most likely reflects the absence of weak intermolecular interactions involving the $[Ni_2(L^2)(\mu\text{-}N_3)]^+$ cation and the other co-crystallized species (H₂O and BPh_4^-). This is further supported by the fact that the $^3A_{2g} \rightarrow {}^3T_{1g}$ (ν_2) (λ_{max} = 646 nm) and $^3A_{2g} \rightarrow {}^1E_g$ (D) (λ_{max} ~ 920 nm) transitions remain unaffected upon dissolving **8**·H₂O in either pure acetonitrile or in a mixture containing 50% of methanol, whereas the broad $^3A_{2g} \rightarrow {}^3T_{2g}$ (ν_1) band undergoes a slight bathochromic shift from 1003 to 1020 nm. In spite of that, it can be safely concluded that the layout of the ligand scaffold in **8**·H₂O remains essentially unchanged upon dissolution, in contrast to **7**·H₂O which undergoes some detectable rearrangements.

Table 2. Spectroscopic Data for Complexes **3**, **7**, and **8** in Solution and in the Solid State (Diffuse Reflectance)[a]

complex	λ_{max}/nm (ε_{max}/M^{-1} cm^{-1}) MeCN/MeOH[b]	λ_{max}/nm (ε_{max}/M^{-1} cm^{-1}) MeCN	λ_{max}/nm Solid state[c]	assignment
3	530 (296)	531 (301)	~ 540 sh	$^3B_1 \rightarrow {}^3E$
	635 (448)	635 (454)	633 (s)	$^3B_1 \rightarrow {}^3B_2$
	786 (111)	786 (110)	791 (w)	$^3B_1 \rightarrow {}^3A_2$
	1012 (38)	1012 (35)	1010 (w)	$^3B_1 \rightarrow {}^3E$
7	644 (63)	645 (54)	673 (m)	$^3A_{2g} \rightarrow {}^3T_{1g}$ (ν_2)
	~ 915 sh (35)	~ 914 sh (34)	~ 935 sh	$^3A_{2g} \rightarrow {}^1E_g$ (D)
	1020 (57)	1020 (57)	1069 (m)	$^3A_{2g} \rightarrow {}^3T_{2g}$ (ν_1)
8	643 (71)	645 (56)	646 (m)	$^3A_{2g} \rightarrow {}^3T_{1g}$ (ν_2)
	~ 915 sh (35)	~ 914 sh (36)	~ 920 sh	$^3A_{2g} \rightarrow {}^1E_g$ (D)
	1021 (56)	1020 (58)	1003 (m)	$^3A_{2g} \rightarrow {}^3T_{2g}$ (ν_1)

[a] UV–vis spectra recorded at ambient temperature. Concentration: 10^{-3} M. [b] MeCN/MeOH (1/1 v/v). [c] Diffuse reflectance data of microcrystalline samples. Intensity: *s* = strong, *m* = medium, *w* = weak; sh denotes a shoulder.

Determination of Stability Constants. According to our former spectrophotometric solution equilibrium studies on halide uptake by complex **3** in MeCN/MeOH (1/1 v/v),[21] azide binding was expected to cause likewise distinct spectral changes in the UV–vis–NIR range due to a change of the coordination geometry from square-pyramidal (N_3S_2 donor set in **3**) to octahedral in the azido-bridged complex **7** ($N_3S_2N_{azide}$ donor environment). For comparison purposes, the same binary solvent mixture as used previously was selected herein too. The incremental addition of up to 2 equiv. of N(*n*-Bu)$_4$N$_3$ to a solution of **3** (eq 3) induces a spontaneous change of the UV absorption features ($250 \leq \lambda \leq 400$ nm) with the progressive disappearance of the shoulder appearing close to 268 nm and the band centered at 319 nm. Concomitantly, a maximum at 299 nm occurs, together with isosbestic points at 286, 316, and 335 nm (Figure 8). In the vis–NIR range, new absorption bands at 646 and 1021 nm characteristic for **7** progressively grow in with increasing N_3^- concentration, while the main

absorption characteristics of **3** (530, 635, 786, 1012 nm) vanish (Table 2). Nonlinear least-squares refinements of the titration data converged for a speciation model involving **3** and its 1:1 azido complex **7** with an association constant of log K_{11} = 5.20(1). Accordingly, ~98% conversion of **3** into adduct **7** is achieved upon addition of 2 equiv. of N_3^- at one millimolar concentration level.

$$\underset{\mathbf{3}}{[Ni_2(L^2)][ClO_4]_2} + N(n\text{-}Bu)_4X \underset{}{\overset{\text{MeCN/MeOH (1/1 v/v)}}{\rightleftharpoons}} \underset{\begin{array}{l}\mathbf{4}\ (X = F^-)\\ \mathbf{5}\ (X = Cl^-)\\ \mathbf{7}\ (X = N_3^-)\end{array}}{[Ni_2(L^2)(\mu_{1,1}\text{-}X)][ClO_4] + N(n\text{-}Bu)_4ClO_4} \quad (3)$$

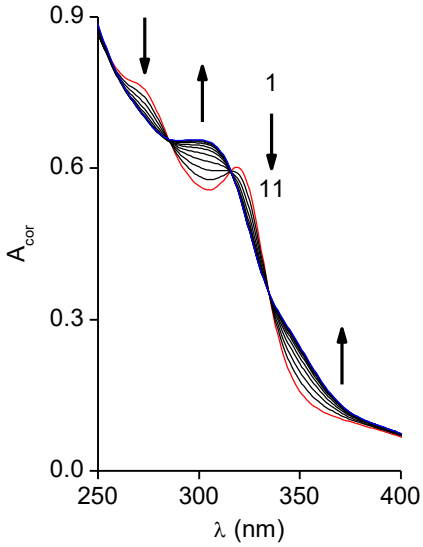

Figure 8. Spectrophotometric titration of the dinickel(II) complex **3** as a function of increasing amounts of $N(n\text{-}Bu)_4N_3$ added in 25 μL increments. Overall, 21 spectra were collected in 0.1 equiv. steps and refined simultaneously, but only one every two curves (corrected for dilution effects) is displayed for sake of clarity. Solvent: MeCN/MeOH (1/1 v/v), I = 0.01 M $N(n\text{-}Bu)_4ClO_4$, T = 298(1) K, $[\mathbf{3}]_0 = 5.02 \times 10^{-5}$ M, $[N(n\text{-}Bu)_4N_3] = 3.40 \times 10^{-4}$ M (spectra 1–11: 0–2 equiv.), V_0 = 1.70 mL.

Compared with our previous findings, the azido-bridged complex is about 1.1 orders of magnitude more stable than the chlorido-bridged $[Ni_2(L^2)(\mu\text{-}Cl)]^+$ analog, but is about 370 times less stable than the fluorido-bridged $[Ni_2(L^2)(\mu\text{-}F)]^+$ species (Table 3).[21] This is also supported by DFT calculations. The computed affinity (E_a, Table 3) of receptor **3** for the N_3^- ion is substantially smaller than the fluorido-bridged complex, while the chlorido-bridged species is less stable than the azido complex. The K_{11} value for the azido complex is also in a typical range for host-guest complexes held together by coordinative bonds. Fabbrizzi and Favarelli, for example, found a log *K* value of ~5.8 for N_3^- binding to a cylindrical dizinc complex supported by a bis(tren) cryptand in water.[17] Diederich has reported a hexaprotonated bis(tren) cryptate that formed a strong 1:1 complex.[38] In water the log *K* value was found to be 4.3.

Table 3. Thermodynamic Parameters for F^-, Cl^-, and N_3^- Uptake by $[Ni_2(L^2)]^{2+}$ (**3**)[a]

anion	complex formed	log K_{11} (UV)	log K_{11} (ITC)	Δ_rG (kJ mol^{-1})	Δ_rH (kJ mol^{-1})	$-T\Delta_rS$ (kJ mol^{-1})	E_a[f] (kJ mol^{-1})
F^-	$[Ni_2(L^2)(\mu\text{-}F)]^+$	7.77(9)[b] 6.94[d]	6.84(7)[c]	–39.0(4)[c]	–5.2(1)[c]	–33.8(8)[c]	90.4
N_3^-	$[Ni_2(L^2)(\mu\text{-}N_3)]^+$	5.20(1)[e] 4.37[d]	4.88(4)[c]	–27.8(2)[c]	–18.8(8)[c]	–9.0(9)[c]	42.7
Cl^-	$[Ni_2(L^2)(\mu\text{-}Cl)]^+$	4.13(3)[b] 3.30[d]	3.52(5)[c]	–20.1(3)[c]	–4.7(2)[c]	–15.4(4)[c]	16.3

[a] Solvent: MeCN/MeOH (1/1 v/v). [b] I = 0.01 M N(*n*-Bu)$_4$ClO$_4$, T = 298(1) K, UV spectrophotometry (190–400 nm), Ref. 21. [c] I = 0.1 M N(*n*-Bu)$_4$ClO$_4$, T = 298.15(2) K, ITC, this work. [d] Estimated value at I = 0.1 M using the Davies equation (eq 4): log K_{11} (I = 0.1) ≈ log K_{11} (I = 0.01) – 0.83, see text for further details. [e] I = 0.01 M N(*n*-Bu)$_4$ClO$_4$, T = 298(1) K, UV spectrophotometry (250–400 nm), this work. [f] Anion affinity of receptor **3** according to PBE0 functional calculations with TZV(P) basis set.

The overall selectivity sequence of **3** for monovalent anions (X^-) is in the order $Br^- < Cl^- < N_3^- < F^-$, and this appears to correlate with the proton affinity of these ions (i.e. gas phase basicities: Br^- = 1354, Cl^- = 1395, N_3^- = 1439, F^- = 1554 kJ/mol),[39,40] as well as with the average Ni–X distances measured on the crystal structures (Ni–X = 2.65 Å for Br^-, 2.47 Å for Cl^-, 2.18 Å for N_3^-, and 2.06 Å for F^-).[21] In other words, the higher the basicity of the anion, the stronger is the binding to **3**. A similar behavior was previously noted for a series of

carboxylato-bridged dinickel(II) complexes supported by the smaller $(L^1)^{2-}$ macrocycle.[41] On the basis of the present data, it is likely that this is a general property of dinickel complexes with a $N_3Ni_2(\mu\text{-}S)_2(\mu\text{-}L)NiN_3$ core supported by aza-thiophenolato donor macrocycles.

The reactions given in eq 3 were also studied by isothermal titration calorimetry (ITC) to get further insights into the thermodynamics of the guest binding by **3**. Figure 9 shows the thermogram and binding isotherm for the titration of $N(n\text{-}Bu)_4N_3$ into a solution of **3** dissolved in the binary solvent mixture MeCN/MeOH (1/1 v/v). The corresponding binding isotherms for the titrations of **3** with F^- and Cl^- are provided in the Supporting Information (Figures S2 and S3, respectively).

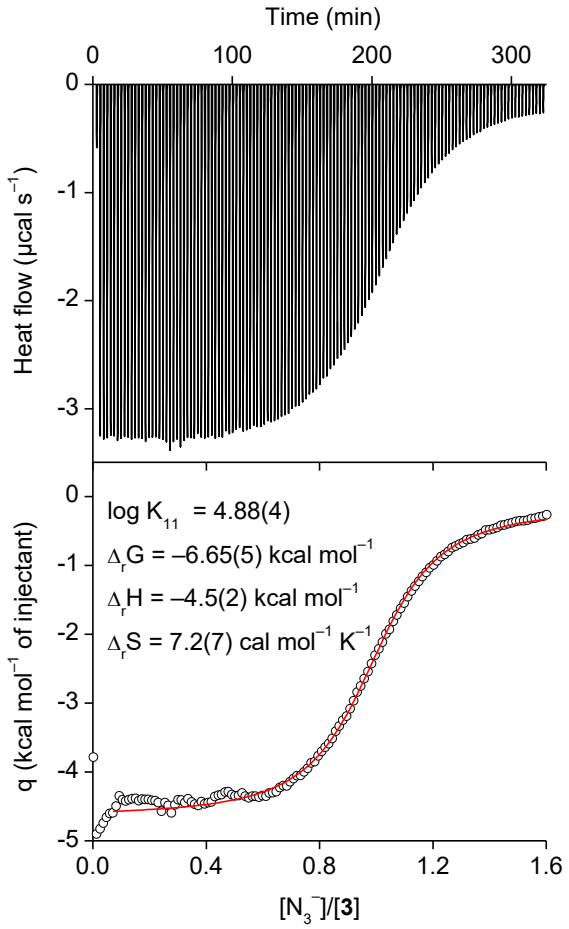

Figure 9. Isothermal calorimetric titration of the dinickel(II) complex **3** as a function of increasing amounts of $N(n\text{-}Bu)_4N_3$ added in 2 µL increments. Solvent: MeCN/MeOH (1/1 v/v), I = 0.1 M $N(n\text{-}Bu)_4ClO_4$, T = 298.15(2) K, $[\mathbf{3}]_0 = 8.5 \times 10^{-4}$ M, $[N(n\text{-}Bu)_4N_3] = 6.81 \times$

10^{-3} M, reequilibration time: 150 s, filter period: 2 s. Raw thermal power data were corrected for dilution effects. The red solid line corresponds to the nonlinear least-squares fit of the data for a 1:1 binding model.

The ITC data collected at a ionic strength of I = 0.1 M using N(*n*-Bu)$_4$ClO$_4$ as supporting electrolyte can all be well modeled by assuming a 1:1 bimolecular reaction. At 298.15(2) K, the complexation free energy $\Delta_r G$ for N_3^- binding, was found to be –27.8(2) kJ mol^{-1}, corresponding to an association constant of log K_{11} = 4.88(4) (Table 3). Analysis of the ITC data sets recorded for binding of F^- and Cl^- to **3** revealed that the F^- ion is bound more strongly than N_3^- ($\Delta_r G$ = –39.0(4) kJ mol^{-1}, log K_{11} = 6.84(7)), while the Cl^- is bound less strongly than N_3^- ($\Delta_r G$ = –20.1(3) kJ mol^{-1}, log K_{11} = 3.52(5)). The deviations of the log K_{11} values derived from ITC measurements from those determined by UV titrations can be traced, at least to some extent, to the differences in the ionic strengths at which the individual experiments were performed (I = 0.01 M in case of UV and I = 0.1 M for ITC). A rough estimate for the magnitude of medium effects can be obtained by applying the Davies equation (eq 4), which is valid up to $I \approx 0.1$ M in water.[42,43]

$$\log K = \log K^0 + \frac{1.824 \cdot 10^6 \Delta z^2}{(\varepsilon T)^{3/2}} \cdot \left(\frac{\sqrt{I}}{1+\sqrt{I}} - 0.3I \right) \quad (4)$$

In eq 4, K and K^0 stand for the equilibrium constant at ionic strength I and infinite dilution, respectively, ε is the dielectric constant (ε = 35.1 for acetonitrile/methanol), T the absolute temperature (T = 298.15 K) and $\Delta z^2 = 1^2 - [2^2 + (-1)^2] = -4$ for the equilibrium $[Ni_2(L^2)]^{2+} + X^- \leftrightarrows [Ni_2(L^2)X]^+$. It follows that log K_{11} (I = 0.1) ≈ log K_{11} (I = 0.01) – 0.83. The stability constants derived from spectrophotometric measurements performed in the presence of 0.01 M supporting electrolyte were corrected for medium effects using the latter formula. These

estimates, which are included in Table 3, can now be directly compared to the experimental values obtained by ITC. The agreement is excellent in case of fluoride and is acceptable for chloride and azide (deviation of 0.22 and 0.51 log unit, respectively).

The ITC data further show that the free enthalpy for azide binding divides into both a favorable enthalpic (Δ_rH = −18.8(8) kJ mol^{-1}) as well as a favorable entropic component ($-T\Delta_rS$ = –9.0(9) kJ mol^{-1}). In this case it is the enthalpic contribution that dominates, which is most likely associated with the smaller solvation enthalpy of this ion. The solvation free energy increases in the order N_3^- < Cl^- < F^-,[44] hence less energy is required to (partially) desolvate N_3^- in order to bind it. The Δ_rH values for F^- (–5.2(1) kJ mol^{-1}) and Cl^- binding (–4.7(2) kJ mol^{-1}) are significantly smaller, a fact which would be consistent with this view. The favorable entropic component is not surprising in view of the crystal structures, which indicate that the halide and azide ions become fully desolvated upon encapsulation into the binding pocket of complex **3**. The $T\Delta_rS$ term clearly increases in the order N_3^- (9.0(9) kJ mol^{-1}) < Cl^- (15.4(4) kJ mol^{-1}) < F^- (33.8(4) kJ mol^{-1}), which further supports the idea that anion desolvation plays a key role in explaining the overall stability of the supramolecular edifice. Moreover, the volume of the cation is increasing upon binding of a substrate while its charge decreases, resulting in a less well solvated complex in media with high dielectric constants (MeOH can probably be considered as such). These two factors are also in favor of positive entropy. To our knowledge, solution thermodynamic data for the nickel(II) azide system have only been determined for aqueous solutions. Ahrland and Avsar have investigated azide binding to $[Ni(H_2O)_6)]^{2+}$.[45] The value of $T\Delta_rS$ = 4.0(2) kJ mol^{-1} is significantly smaller than in our case, as should be expected for an unconstrained reaction in which desolvation of the azide ion is less pronounced.

Conclusion

The azido-bridged dinickel(II) complex $[Ni_2(L^2)(\mu_{1,1}\text{-}N_3)]^+$ supported by the 28-membered hexaza-dithiophenolate macrocycle is readily prepared by reaction of its precursor $[Ni_2(L^2)][ClO_4]_2$ (**3**) with N_3^- and can be isolated as an air-stable perchlorate $[Ni_2(L^2)(\mu_{1,1}\text{-}N_3)][ClO_4]$ (**7**) or tetraphenylborate $[Ni_2(L^2)(\mu_{1,1}\text{-}N_3)][BPh_4]$ (**8**) salt. The two compounds bind the N_3^- ion specifically in the *end-on* mode, which is in stark contrast to the *end-to-end* coordination encountered for the related azido complex $[Ni_2(L^1)(\mu_{1,3}\text{-}N_3)][ClO_4]$ (**2**) of the smaller 24-membered macrocycle $(L^1)^{2-}$. This is attributed to a higher degree of pre-organization, as manifested by the number of possible macrocyclic conformations (one for complexes **3**–**8** denoted as type C vs. two for complexes **1** and **2** of type A and B, respectively), but also to repulsive interactions between the azide ion and the propylene groups of the macrocycle. The switch of the coordination mode from *end-to-end* in **2** to *end-on* in **7** and **8** also affects the magnetic exchange interactions. In contrast to $[Ni_2(L^1)(\mu_{1,3}\text{-}N_3)][ClO_4]$ (**2**), which features a $S = 0$ ground state, $[Ni_2(L^2)(\mu_{1,1}\text{-}N_3)][BPh_4]$ (**8**) has a $S = 2$ ground state that is attained by competing antiferromagnetic and ferromagnetic exchange interactions via the thiolato- and azido bridges with a value for the magnetic exchange coupling constant J of 13 cm^{-1} ($\mathbf{H} = -2JS_1S_2$). According to ITC measurements performed in MeCN/MeOH 1/1 v/v at $I = 0.1$ M $N(n\text{-}Bu)_4ClO_4$ and $T = 298.15(2)$ K, the stability of the azido-bridged complex ($\log K_{11} = 4.88(4)$) was found to lie in between those of the fluorido- ($\log K_{11} = 6.84(7)$) and chlorido-bridged complexes ($\log K_{11} = 3.52(5)$), correlating with the proton affinity of these ions. The free energy for binding of azide divides into both favorable enthalpic ($\Delta_rH = -18.8(8)$ kJ mol^{-1}) and entropic components ($-T\Delta_rS = -9.0(9)$ kJ mol^{-1}). In contrast to F^- and Cl^-, it is the enthalpic contribution that dominates for N_3^- binding, which is most likely associated with the smaller solvation enthalpy of this ion.

Experimental Section

Materials and Methods. Compound **3**·2H_2O was prepared as described in the literature.[21] The synthesis of the metal complexes was carried out under a protective atmosphere of argon. Melting points were determined in open-glass capillaries and are uncorrected. Mid infrared spectra (4000–400 cm^{-1}) were recorded at 4 cm^{-1} resolution on a Bruker TENSOR 27 (KBr pellets) or a VERTEX70v FT-IR spectrometer, the latter being equipped with an A225 diamond ATR accessory from Bruker. Raman spectra were acquired with a Renishaw inVia spectrometer equipped with a 632.8 nm He-Ne laser excitation source, an 1800 grooves/mm grating, and a microscope fitted with a ×50 objective. Wavenumbers were calibrated with respect to the silicon scattering line at 520(1) cm^{-1} of an internal standard, whereas an external Si reference was used periodically to check for energy drifts over time. Solution absorption spectra were collected on a Jasco V-670 UV–vis–NIR spectrophotometer using 1 cm quartz cells (Hellma). Diffuse reflectance spectra of microcrystalline complexes dispersed in dry barium sulfate (Avocado, <99%) were acquired between 200 and 2500 nm on a Cary 5000 (Agilent) UV–vis–NIR spectrophotometer fitted with a DRA-2500 integration sphere (Labsphere), the baseline being recorded on $BaSO_4$. Corrected reflectance data were converted to $f(R)$ values using the Kubelka-Munk function expressed as $f(R) = (1 - R)^2/2R$. ESI mass spectra were recorded on a Bruker Daltronics APEX II spectrometer. Elemental analyses were carried out on a VARIO EL elemental analyzer (Elementar Analysensysteme GmbH, Hanau). Temperature-dependent magnetic susceptibility measurements on powdered solid samples were carried out using a MPMS 7XL SQUID magnetometer (Quantum Design) over the temperature range 2–330 K at an applied magnetic field of 0.5 Tesla. The observed susceptibility data were corrected for underlying diamagnetism.

CAUTION! *Perchlorate salts, azide salts, and azide complexes are potentially explosive and should therefore be prepared only in small quantities and handled with appropriate care.*

[Ni$_2$(L^2)($\mu_{1,1}$-N$_3$)][ClO$_4$]·H$_2$O (7·H$_2$O). To a solution of [Ni$_2$(L^2)][ClO$_4$]$_2$·2H$_2$O (**3**·2H$_2$O) (98.6 mg, 0.096 mmol) in MeOH (50 mL) was added a solution of N(*n*-Bu)$_4$N$_3$ (31.3 mg, 0.11 mmol) in MeOH (5 mL) at room temperature, resulting in an immediate color change from dark green to bright green. The reaction mixture was stirred for about 30 min after which a solution of LiClO$_4$·3H$_2$O (160 mg, 1.00 mmol) in ethanol (20 mL) was added. The solution was concentrated under reduced pressure until bright-green crystals formed, which were filtered, washed with cold ethanol, and dried in vacuum. The crude product was purified by recrystallization from a mixed acetonitrile/ethanol solution. Yield: 81 mg (87%). mp > 251 °C (decomposes without melting). IR (KBr, cm^{-1}): $\tilde{\nu}$ = 3441 (s), 3304 (m), 3272 (s), 2953 (s), 2863 (s), 2040 (vs, ν_{asym}(N$_3$)), 1630 (m), 1476 (s), 1450 (s), 1393 (m), 1377 (m), 1361 (s), 1288 (s), 1271 (m), 1240 (m), 1226 (m), 1203 (m), 1188 (m), 1156 (s), 1121 (s), 1102 (s), 1084 (s), 1063 (s), 1051 (m), 1006 (s), 981 (m), 954 (m), 928 (m), 905 (m), 872 (s), 857 (m), 816 (m), 806 (m), 796 (w), 754 (m), 742 (m), 673 (m), 621 (s), 599 (w), 512 (w), 497 (w), 410 (w). IR (ATR, cm^{-1}): $\tilde{\nu}$ = 2038 (vs, ν_{asym}(N$_3$)). Raman (cm^{-1}): $\tilde{\nu}$ = 1297 (ν_{sym}(N$_3$)). (+)-ESI-MS: *m/z* (CH$_3$CN) = 826.3 [M–ClO$_4$]$^+$. UV–vis (MeCN): λ_{max} / nm (ε / M^{-1} cm^{-1}) = 197 (70270), 300 (13477), 645 (54), 1020 (57). Anal. calcd (%) for C$_{38}$H$_{64}$ClN$_9$Ni$_2$O$_4$S$_2$·H$_2$O (927.94 + 18.02): C 48.25, H 7.03, N 13.33; found: C 48.68, H 6.71, N 13.21.

[Ni$_2$(L^2)($\mu_{1,1}$-N$_3$)][BPh$_4$]·H$_2$O (8·H$_2$O). To a solution of [Ni$_2$(L^2)($\mu_{1,1}$-N$_3$)][ClO$_4$]·H$_2$O (**7**·H$_2$O) (92.8 mg, 0.098 mmol) in MeOH (50 mL) was added a solution of NaBPh$_4$ (342 mg, 1.00 mmol) in EtOH (10 mL). After stirring for 10 min at room temperature, the solution was concentrated under reduced pressure until bright green crystals formed, which were filtered, washed with cold ethanol, and dried in vacuum. The crude product was purified by recrystallization from a mixed acetonitrile/ethanol solution. Yield: 108 mg (94%). mp > 233 °C (decomposes without melting). IR (KBr, cm^{-1}): $\tilde{\nu}$ = 3281 (w), 3241 (m), 3054 (m), 2964

(s), 2859 (s), 2041 (vs, $\nu_{asym}(N_3)$), 1580 (m), 1436 (s), 1360 (m), 1291 (m), 1228 (m), 1154 (s), 1084 (m), 1052 (m), 977 (m), 919 (m), 871 (s), 814 (w), 741 (s), 707 (s), 611 (m). IR (ATR, cm^{-1}): $\tilde{\nu}$ = 2035 (vs, $\nu_{asym}(N_3)$). Raman (cm^{-1}): $\tilde{\nu}$ = 1303 ($\nu_{sym}(N_3)$). (+)-ESI-MS: *m/z* (CH_3CN) = 826.3 $[M–BPh_4]^+$. UV–vis (MeCN): λ_{max} / nm (ε / M^{-1} cm^{-1}) = 199 (168085), 303 (14079), 645 (56), 1020 (58). Magnetic moment at 290 K: $\mu_{eff,dim}$ = 4.4 μ_B (per binuclear unit), μ_{eff} = 3.12 μ_B (per Ni^{2+})). Anal. calcd (%) for $C_{62}H_{84}BN_9Ni_2S_2 \cdot H_2O$ (1147.72 + 18.02): C 63.88, H 7.44, N 10.81; found: C 64.02, H 7.30, N 10.74.

Crystallography. Single crystals of $[Ni_2(L^2)(\mu\text{-}N_3)][ClO_4]\cdot 5EtOH$ (**7**·5EtOH) suitable for X-ray crystallography were obtained by slow evaporation of a mixed methanol/ethanol (1/1 v/v) solution of **7**. The crystals quickly lose the solvate molecules upon standing in air and turn dull. The diffraction experiment was carried out at 213 K on a STOE IPDS-2T X-ray diffractometer. The intensity data were processed with the program STOE X-AREA.[46] The structure was solved by direct methods[47] and refined by full-matrix least-squares on the basis of all data against F^2 using SHELXL-97.[48] PLATON was used to search for higher symmetry.[26] H atoms were placed in calculated positions and treated isotropically using the 1.2-fold U_{iso} value of the parent atom, excepted for methyl protons which were assigned the 1.5-fold U_{iso} value of the parent C atoms. Unless otherwise noted, all non-hydrogen atoms were refined anisotropically. ORTEP-3 was used for the artwork of the structures.[49]

Crystal Data for $[Ni_2(L^2)(\mu_{1,1}\text{-}N_3)][ClO_4]\cdot 5EtOH$ (7·5EtOH). $C_{38}H_{66}ClN_9Ni_2O_5S_2$, M_r = 945.99 g/mol, monoclinic space group $P2_1/c$, a = 16.929(3) Å, b = 23.299(5) Å, c = 13.836(3) Å, β = 105.73(3)°, V = 5253(2) $Å^3$, Z = 4, ρ_{calcd} = 1.196 g/cm^3, T = 213 K, μ(Mo K_α) = 0.891 mm^{-1} (λ = 0.71073 Å), 33740 reflections measured, 9228 unique, 6407 with $I > 2\sigma(I)$. Final R_1 = 0.0449, wR_2 = 0.1190 ($I > 2\sigma(I)$), 505 parameters and 42 restraints, min./max. residual

electron density = –0.660/0.738 e/Å^3. The five ethanol molecules are heavily disordered and were therefore removed from the structure (and the corresponding F_o) with the SQUEEZE procedure implemented in the PLATON program suite.[26] Removing the five ethanol molecules led to a total solvent accessible void of 1290 Å^3, in good agreement with the space needed by five ethanol molecules. The perchlorate ion was found to be disordered over two positions. A split atom model with fixed site occupancy factors could be applied to account for this disorder.

Computational Details. All calculations were performed using density functional theory (DFT) within the broken symmetry approach.[50,51] The hybrid functional of Perdew, Burke and Ernzerhof (PBE0)[52,53] and Ahlrichs triple-zeta valence basis set (TZV(P))[54] as implemented in the ORCA[55,56] program package (revision 2.80) have been used for all calculations. The geometry of all considered structures were taken from the crystal structures and were fixed during the calculations. Relativistic effects have been incorporated by zero-order regular approximation (ZORA).[57] The calculation of *J* included the following steps: definition of the geometry of the molecule from X-ray analysis; calculation of the total energy for the high-spin (HS) state (S = 2); calculation of the total energy for the broken-symmetry (BS) state (S = 0); calculation of the J value within the following scheme:

$$J = \frac{^{BS}E(X) - ^{HS}E(X)}{^{HS}\langle S^2\rangle - ^{BS}\langle S^2\rangle}. \qquad (5)$$

where ^{HS}E, $^{HS}\langle S^2\rangle$ correspond to the total energy and total spin angular momentum for the high-spin state (HS), ^{BS}E and $^{BS}\langle S^2\rangle$ to the total energy and total spin angular momentum for the broken-symmetry state (BS). This scheme is valid over the whole coupling strength regime.[58] The calculation of the azide ion affinity $E_a(N_3^-)$ was carried out according to (Eq 6), in a manner analogous to the computation of the halide ion affinities.[21] $^{HS}E([Ni_2(L^{Me2H4})(\mu$-

$N_3^-)]^+$) represents the total energy of the complex **7** in its high-spin state, ^{BS}E(**3**) the total energy of $[Ni_2(L^{Me2H4})]^{2+}$ (low-spin state), and $E(N_3^-)$ the total energy of the azide ion.

$$E_a(N_3^-) = {}^{HS}E(\mathbf{7}]^+) - {}^{BS}E(\mathbf{3}) - E(N_3^-) \quad (6)$$

Spectrophotometric Titrations. All mother solutions were prepared by dissolving carefully weighted (balance accuracy: ± 0.1 mg) materials in the HPLC-grade MeCN/MeOH (1/1 v/v) solvent mixture (VWR BDH Prolabo, HiPerSolv CHROMANORM). Titrations were carried out in a quartz cell (Hellma 110-QS) of 1 cm optical path length containing 1.7 mL of a $[Ni_2(L^2)][ClO_4]_2{\cdot}2H_2O$ (**3**·$2H_2O$) stock solution (5.02×10^{-5} M) and 0.1 M N(*n*-Bu)$_4ClO_4$ as supporting electrolyte. Aliquots of 25 μL of an N(*n*-Bu)$_4N_3$ solution were added with an Eppendorf micropipette (volume range 10–100 μL; 3.0–0.8% error). UV absorption spectra were collected in the 250–400 nm range at uniform data point interval of 1 nm with a double-beam V-670 (Jasco) spectrophotometer, which is certified by the manufacturer to have a linear response up to 6 AU. Moreover, it was ascertained that solutions of complex **3** obey to the Lambert-Beer law up to 10^{-2} M. Equilibration time between each incremental addition was found to be fast, as identical spectra were obtained by cycling the recordings with a 4 min delay between two consecutive measurements.

The multiwavelength data sets were analyzed by the HypSpec 2014 software.[59] The goodness-of-fit was assessed by the overall standard deviation (σ), the visual inspection of the residuals, and by the physical meaning of the calculated electronic absorption spectra. Unless otherwise noted (standard deviation on the arithmetic mean), the reported uncertainties correspond to the standard deviation of the refined parameters that were returned by the fitting software. Species distribution calculations were performed with the program Hyss.[60]

Isothermal Titration Calorimetry. Association constants were determined using a VP-ITC isothermal titration microcalorimeter (MicroCal part of Malvern Instruments Ltd, Worcestershire, UK) at 25 °C by measuring the heat released during reaction of **3** with the respective co-ligands. A 0.1 M N(*n*-Bu)$_4$ClO$_4$ solution in the degassed mixed solvent system MeCN/MeOH (1/1 v/v) was used as the supporting electrolyte. Starting volume in the cell was 1425 μL. The stirring speed was set to 306 rpm and the reference power to 20 μcal/s. The injection syringe had a maximum loading volume of 280 μL. To avoid contamination, the ITC sample cell was filled at least five times with acetonitrile, thoroughly flushed with 300 mL methanol, and dried by air suction for 20 min. Raw thermal power data were corrected for dilution effects and analyzed with a combination of the software programs NITPIC (release 1.0.4b)[61] and SEDPHAT (release 10.58d).[62] The complex concentrations were adjusted so that the inflection point of the integrated thermogram coincided with a molar concentration ratio [N_3^-]/[**3**] of 1.

Supporting Information

Table of selected bond lengths and angles for **3**·4EtOH, **7**·5EtOH, and **2**·3MeOH. Diffuse reflectance spectra of microcrystalline samples of **3**·2H$_2$O, **7**·H$_2$O, and **8**·H$_2$O. ITC data for the reaction of **3**·2H$_2$O with N(*n*-Bu)$_4$F and N(*n*-Bu)$_4$Cl. Electrospray ionization mass spectra of **7**·H$_2$O and **8**·H$_2$O. This material is available free of charge via the Internet at http://pubs.acs.org. CCDC-1437970 contains the supplementary crystallographic data for this paper. These data can be obtained free of charge from the Cambridge Crystallographic Data Centre via www.ccdc.cam.ac.uk/data_request/cif.

Acknowledgments

Financial support from the Deutsche Forschungsgemeinschaft DFG-FOR 1154 "Towards molecular spintronics", the Universität Leipzig, the Centre National de la Recherche

Scientifique (CNRS), and the Conseil Régional de Bourgogne (PARI II-CDEA program) is gratefully acknowledged. We thank Prof. Dr. Norbert Sträter for providing facilities for ITC measurements, Michel Krauss for assistance with the measurements, and Dr Christine Stern (ICMUB) for acquiring the Raman spectra.

References

(1) Pierpont, C. G.; Hendrickson, D. N.; Duggan, D. M.; Wagner, F.; Barefield, E. K. *Inorg. Chem.* **1975**, *14*, 604–610.

(2) (a) Charlot, M. F.; Kahn, O.; Chaillet, M.; Larrieu, C. *J. Am. Chem. Soc.* **1986**, *108*, 2574–2581. (b) Bencini, A.; Ghilardo, C. A.; Midollini, S.; Orlandini, A. *Inorg. Chem.* **1989**, *28*, 1958–1962. (c) Escuer, A.; Vicente, R.; Ribas, J.; Salah El Fallah, M.; Solans, X.; Font-Bardía, M. *Inorg. Chem.* **1994**, *33*, 1842−1847.

(3) Ribas, J.; Escuer, A.; Monfort, M.; Vicente, R.; Cortes, R.; Lezama, L.; Rojo, T. *Coord. Chem. Rev.* **1999**, *193-195*, 1027−1068.

(4) Halcrow, M. A.; Huffman, J. C.; Christou, G. *Angew. Chem.* **1995**, *107*, 971−973; *Angew. Chem. Int. Ed. Engl.* **1995**, *34*, 889–891.

(5) Meyer, F.; Kircher, P.; Pritzkow, H. *Chem. Commun.* **2003**, 774–775.

(6) (a) Papaefstathiou, G. S.; Perlepes, S. P.; Escuer, A.; Vicente, R.; Font-Bardia, M.; Solans, X. *Angew. Chem.* **2001**, *113*, 908–910; *Angew. Chem., Int. Ed.* **2001**, *40*, 884–886. (b) Papaefstathiou, G. S.; Escuer, A.; Vicente, R.; Font-Bardia, M.; Solans, X.; Perlepes, S. P. *Chem. Commun.* **2001**, 2414–2415.

(7) Demeshko, S.; Leibeling, G.; Maringgele, W.; Meyer, F.; Mennerich, C.; Klauss, H.-H.; Pritzkow, H. *Inorg. Chem.* **2005**, *44*, 519–528.

(8) Sasmal, S.; Hazra, S.; Kundu, P.; Majumder, S.; Aliagla-Alcalde, N.; Ruiz, E.; Mohanta, S. *Inorg. Chem.* **2010**, *49*, 9517–9526.

(9) (a) Tandon, S. S.; Bunge, S. D.; Rakosi, R.; Xu, Z.; Thompson, L. K. *Dalton Trans.* **2009**, 6536–6551. (b) Tandon, S. S.; Bunge, S. D.; Sanchiz, J.; Thompson, L. K. *Inorg. Chem.* **2009**, 6536–6551.

(10) Chaudhuri, P.; Weyhermüller, T.; Bill, E.; Wieghardt, K. *Inorg. Chim. Acta* **1996**, *252*, 195–202.

(11) Ribas, J.; Monfort, M.; Gosh, B. K.; Solans, X. *Angew. Chem.* **1994**, *106*, 2177–2179; *Angew. Chem., Int. Ed. Engl.* **1994**, *33*, 2087–2089.

(12) Vicente, R.; Escuer, A.; Ribas, J.; Salah El Fallah, M.; Solans, X.; Font-Bardía, M. *Inorg. Chem.* **1993**, *32*, 1920–1924.

(13) Colacio, E.; Costes, J.-P.; Domínguez-Vera, J. M.; Ben Maimounac, I.; Suárez-Varela, J. *Chem. Commun.* **2005**, 534–536.

(14) Beer, P. D.; Drew, M. G. B.; Leeson, P. B.; Lyssenko, K.; Odgen, M. I. *J. Chem. Soc., Chem. Commun.* **1995**, 929–930.

(15) Chauduri, P.; Guttmann, M.; Ventur, D.; Wieghardt, K.; Nuber, B.; Weiss, J. *J. Chem. Soc., Chem. Commun.* **1985**, 1618–1620.

(16) (a) Escuer, A.; Harding, C. J.; Dussart, Y.; Nelson, J.; McKee, V.; Vicente, R. *J. Chem. Soc., Dalton Trans.* **1999**, 223–227. (b) Harding, C. J.; Mabbs, F. E.; MacInnes, E. J. L.; McKee, V.; Nelson, J. *J. Chem. Soc., Dalton Trans.* **1996**, 3227–3230.

(17) Fabbrizzi, L.; Favarelli, I. *Chem. Commun.* **1998**, 971–972.

(18) Lozan, V.; Loose, C.; Kortus, J.; Kersting, B. *Coord. Chem. Rev.* **2009**, *253*, 2244–2260.

(19) Kersting, B.; Steinfeld, G. *Chem. Commun.* **2001**, 1376–1377.

(20) Hausmann, J.; Klingele, M.-H.; Lozan, V.; Steinfeld, G.; Siebert, D.; Journaux, Y.; Girerd, J.-J.; Kersting, B. *Chem. Eur. J.* **2004**, *10*, 1716–1728.

(21) Jeremies, A.; Lehmann, U.; Gruschinski, S.; Schleife, F.; Meyer, M.; Matulis, V.; Ivashkevich, O. A.; Handke, M.; Stein, K.; Kersting, B. *Inorg. Chem.* **2015**, *54*, 3937−3950.

(22) The non-methylated derivative of $(L^2)^{2-}$ does not support any triply-bridged structures at all, see: Lehmann, U.; Lach, J.; Loose, C.; Kortus, J.; Kersting, B. *Dalton Trans.* **2013**, *42*, 987–996.

(23) Bondi, A. *J. Phys. Chem.* **1964**, *68*, 441–451.

(24) (a) Brammer, L.; Bruton, E. A.; Sherwood, P. *Cryst. Growth Des.* **2001**, *4*, 277–290. (b) Mascal, M.; Armstrong, A.; Bartberger, M. D. *J. Am. Chem. Soc.* **2002**, *124*, 6274–6276.

(25) Pascal, R. A. *Eur. J. Org. Chem.* **2004**, 3763–3771.

(26) Spek, A. L. *PLATON − A Multipurpose Crystallographic Tool*; Utrecht University: Utrecht, The Netherlands, 2000.

(27) Tachikawa, T.; Ramaraj, R.; Fujitsuka, M.; Majima, T. *J. Phys. Chem. B* **2005**, *109*, 3381−3386.

(28) Ginsberg, A. P.; Brookes, R. W.; Martin, R. L.; Sherwood, R. C. *Inorg. Chem.* **1972**, *11*, 2884–2889.

(29) O'Connor, C. J. *Prog. Inorg. Chem.* **1982**, *29*, 203–283.

(30) Kahn, O. *Molecular magnetism*; VCH: Weinheim, 1993.

(31) Herchel, R.; Boca, R.; Krzystek, J.; Ozarowski, A.; Duran, M.; van Slageren, J.; *J. Am. Chem. Soc.* **2007**, *129*, 10306−10307.

(32) Azuah, R. T.; Kneller, L.R.; Qiu, Y.; Tregenna-Piggott, P. L. W.; Brown, C. M.; Copley, J. R. D.; Dimeo, R. M. J. *J. Res. Natl. Inst. Stand. Technol.* **2009**, *114*, 341–358.

(33) The *D* values should be taken as indicative rather than definitive, because temperature dependent magnetic susceptibility measurements are not very appropriate for the determination of *D* values. Meyer, A.; Gleizes, A.; Girerd, J.-J.; Verdaguer, M.; Kahn, O. *Inorg. Chem.* **1982**, *21*, 1729−1739.

(34) Sasmal, S.; Hazra, S.; Kundu, P.; Dutta, S.; Rajaraman, G.; Sañudo, E. C.; Mohanta, S. *Inorg. Chem.* **2011**, *30*, 7527−7267.

(35) Ruiz, E.; Cano, J.; Alvarez, S.; Alemany, P. *J. Am. Chem. Soc.* **1998**, *120*, 11122–11129.

(36) Nakamoto, K. *Infrared and Raman Spectra of Inorganic and Coordination Compounds*, 6th ed; Wiley: New York, 2009, Part B, p 129−131.

(37) (a) Cortes, R.; Ruiz de Larramandi, J. I.; Lezama, L.; Rojo, T.; Urtiaga, K.; Arriortua, M. I. *J. Chem. Soc., Dalton Trans.* **1992**, 2723–2728. (b) Sasmal, S.; Hazra, S.; Kundu, P.; Majumder, S.; Aliaga-Alcalde, N.; Ruiz, E.; Mohanta, S. *Inorg. Chem.* **2010**, *49*, 9517–9526.

(38) Diederich, B.; Guilhelm, J.; Lehn, J.-M.; Pascard, C.; Sonveaux, E. *Helv. Chim. Acta* **1984**, *67*, 91−104.

(39) Bartmess, J. E.; Scott, J. A.; McIver, R. T. *J. Am. Chem. Soc.* **1979**, *101*, 6046−6056.

(40) Huheey, J.; Keiter, E.; Keiter, R. *Anorganische Chemie*, 2nd ed; de Gruyter: Berlin, 1995.

(41) Lehmann, U.; Klingele, J.; Lozan, V.; Steinfeld, G.; Klingele, M. H.; Käss, S.; Rodenstein, A.; Kersting, B. *Inorg. Chem.* **2010**, *49*, 11018–11029.

(42) Davies, C. W. *Ion Association*; Butterworths: London, 1962.

(43) Vacek Chocholoušová, J.; Vacek, J.; Andronova, A.; Míšek, J.; Songis, O.; Šámal, M.; Stará, I. G.; Meyer, M.; Bourdillon, M.; Pospíšil, L.; Starý, I. *Chem. Eur. J.* **2014**, *20*, 877–893.

(44) For solvation free energies of these anions in different solvents, see: (a) Böes, E. S.; Livotto, P. R.; Stassen, H. *Chem. Phys.* **2006**, *331*, 142−158. (b) Kelly, C. P.; Cramer, C. J.; Truhlar, D. G. *J. Phys. Chem. B* **2006**, *110*, 16066−16081. (c) Pliego, J. R.; Miguel, E. L. M. *J. Phys. Chem. B* **2013**, *117*, 5129–5135.

(45) Ahrland, S.; Avsar, E. *Acta. Chem. Scand.* **1975**, *A29*, 881−889.

(46) Stoe & Cie. *X-AREA* and *X-RED32*; Stoe & Cie GmbH: Darmstadt, Germany, 2012.

(47) Sheldrick, G. M. *Acta Crystallogr., Sect. A.* **1990**, *46*, 467–473.

(48) Sheldrick, G. M. *SHELXL-97*, Computer program for crystal structure refinement; University of Göttingen: Göttingen, Germany, 1997.

(49) Farrugia, L. J. *J. Appl. Crystallogr.* **1997**, *30*, 565–568.

(50) (a) Noodleman, L. *J. Chem. Phys.* **1981**, *74*, 5737–5743. (b) Noodleman, L.; Davidson, E. R. *Chem. Phys.* **1986**, *109*, 131–143.

(51) Noodleman, L.; Peng, C.Y.; Case, D. A.; Mouesca, J. M. *Coord. Chem. Rev.* **1995**, *144*, 199–244.

(52) Perdew, J.; Burke, K.; Ernzerhof, M. *Phys. Rev. Lett.* **1997**, *78*, 1396.

(53) Adamo, C.; Barone, V. *J. Chem. Phys.* **1999**, *110*, 6158–6169.

(54) Schaefer, A.; Horn, H.; Ahlrichs, R. *J. Chem. Phys*. **1992**, *97*, 2571–2577.

(55) Neese, F. *J. Chem. Phys.* **2003**, *119*, 9428–9444.

(56) Neese, F. *Int. J. Quantum Chem.* **2001**, *83*, 104–114.

(57) van Wüllen, C. *J. Chem. Phys.* **1998**, *109*, 392–399.

(58) Soda, T.; Kitagawa, Y.; Onishi, T.; Takano, Y.; Shigeta, Y.; Nagao, H.; Yoshioka, Y.; Yamaguchi, K. *Chem. Phys. Lett.* **2000**, *319*, 223–230.

(59) (a) Gans, P.; Sabatini, A.; Vacca, A. *Talanta* **1996**, *43*, 1739–1753. (b) Gans, P.; Sabatini, A.; Vacca, A. *Ann. Chim. (Rome)* **1999**, *89*, 45–49.

(60) Alderighi, L.; Gans, P.; Ienco, A.; Peters, D.; Sabatini, A.; Vacca, A. *Coord. Chem. Rev*. **1999**, *184*, 311–318.

(61) Keller, S.; Vargas, C.; Zhao, H.; Piszczek, G.; Brautigam, C. A.; Schuck, P. *Anal. Chem.* **2012**, *84*, 5066–5073.

(62) Houtman, J. C. D.; Brown, P. H.; Bowden, B.; Yamagushi, H.; Appella, E.; Samelson, L. E.; Schuck, P. *Protein Sci.* **2007**, *16*, 30–42.

For Table of Contents Only

The binuclear Ni(II) complex $[Ni_2(L^2)(\mu_{1,1}\text{-}N_3)][ClO_4]$ (**7**) binds the N_3^- ion *end-on*, which is in striking contrast to the *end-to-end* coordination encountered for the related azido complex $[Ni_2(L^1)(\mu_{1,3}\text{-}N_3)][ClO_4]$ (**2**) of the smaller macrocycle $(L^1)^{2-}$. This can be traced to a more pre-organized binding pocket, which controls the azide binding mode by repulsive CH···π interactions. Upon going from **2** to **7**, the spin ground state changes from $S = 0$ to $S = 2$.

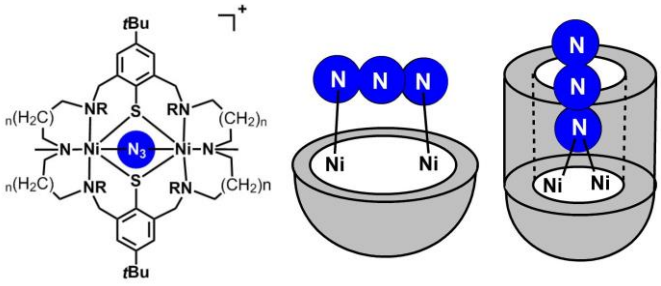

$[Ni_2(L)(N_3)]^+$ **2** (n = 0) **7** (n = 1)